Secondary-electron emission spectroscopy and the observation of high-energy excited states in graphite: Theory and experiment

R. F. Willis and B. Fitton
Surface Physics Division, European Space Research Organisation, Noordwijk, Holland

G. S. Painter*
Metals and Ceramics Division, Oak Ridge National Laboratory, Oak Ridge, Tennessee 37830
(Received 3 April 1973; revised manuscript received 2 August 1973)

Fine structure in the energy distribution of secondary electrons "back-scattered" from a graphite crystal surface is resolved and shown to be a consequence of inelastic electron-electron scattering in which the dominant process is the population of final states above the vacuum level by electron-hole pair production via screened-Coulombic interaction between the incident primary electrons and the valence electrons in the solid. The scattering theory of Kane is applicable and emphasizes that features due to one-electron density of final states should be resolvable in experimental secondary-electron-emission spectra of crystals. Experimental results are presented, which provide strong support for this view. Previous measurements on graphite have been extended and weak secondary-electron-emission structure, resolved in the second derivative of the energy-distribution spectrum, is reported for kinetic energies, $10 \lesssim E_{\rm kin} \lesssim 40$ eV. Maxima are observed at 16.2, 22.2, 29.2, 31.2, 36.2, and 40.7 ± 0.5 eV above the Fermi energy. Details are presented of a first-principles high-energy band-structure calculation of graphite extending over a 80-eV energy range. The observed spectral features correlate closely with final-density-of-states maxima as predicted by the theory.

I. INTRODUCTION

The energy distribution of secondary electrons, emitted into vacuum from solids under bombardment by fast primary electrons, was first described satisfactorily by Wolff[1] as a "cascade" process. Excited electrons are produced internally by the scattered primary beam and diffuse to the surface, multiplying and losing energy en route, and are emitted providing they possess sufficient energy to overcome the surface potential barrier. This, and subsequent theories,[2] predict an energy distribution curve which peaks at low kinetic energies, $E_{\rm kin} \simeq 2$–5 eV, and decreases smoothly at higher energies (the so-called "slow" or "true" secondary peak extending $0 \leq E_{\rm kin} \lesssim 50$ eV). Calculations have been made mainly for scattering by conduction electrons in free-electron solids only, but the "cascade peak" is a common feature of all materials studied to date.[2]

No satisfactory theoretical explanation has been provided, however, for the additional weak fine structure, which has been observed in many cases[3] superimposed on the smoothly varying cascade background. Based on a suggestion originally proposed by Lander,[4] Harrower[5] interpreted structure in the energy distribution of secondaries emitted from tungsten and molybdenum surfaces at energies, $E_{\rm kin} < 50$ eV, to be associated with Auger-electron emission due to the relaxation of holes created in inner-core levels located 20–50 eV below the Fermi level E_F. Similar structure was subsequently observed in the secondary-electron-emission (SEE) spectrum of the lighter elements, but at low primary-beam energies below the ionization threshold for the inner-core levels. Again based on Lander's original suggestion, Scheibner and Tharp[6] conjectured that such structure was a consequence of the population of final states located above the vacuum level E_v, attributable to single-electron $\vec{k}$-conserving interband transitions and to Auger relaxation processes between the holes remaining in the valence band. The excited electrons were assumed to be emitted without further elastic or inelastic scattering. Some support for this viewpoint was provided by later more detailed measurements on well-resolved fine structure in the SEE distribution of graphite.[7] For kinetic energies, $E_{\rm kin} \lesssim 20$ eV, weak maxima in the energy distribution curve were found to correlate closely with emission from density-of-final-states maxima located about critical points in the second Brillouin zone, as predicted by the nonempirical band structure of Painter and Ellis.[8] Furthermore, sharp variations of peak intensities were observed for primary beam energies close to interband thresholds ($E_p = 10$–50 eV) and with angle of incidence of the primary beam, indicative of direct k-conserving "optical"-type transitions obeying the selection rules predicted for this material.[9]

Von Koch,[10] however, reported discrete maxima in the low-energy region of the SEE spectrum of aluminum, which he attributed to single-electron excitations due to electrons at the Fermi level gaining energy from decaying volume and surface plasmons of energies $\hbar\omega_v$ and $\hbar\omega_s$, produced initial-

ly by the primary beam interaction with the solid. This explanation has since been disputed[11] in view of the fact that the observed maxima occurred at kinetic energies equal to the plasmon energies $\hbar\omega_v$ and $\hbar\omega_s$ when no correction was made for the work function of the sample, ϕ_s. An alternative explanation, [11] based on the assumption that the "hot" secondary electrons can lose energy during the escape process by coupling to discrete plasmon excitations, giving rise to discontinuities in the slope of the cascade background curve at $E_{kin} \simeq \hbar\omega_s - \phi_s$ and $E_{kin} \simeq \hbar\omega_v - \phi_s$, rather than discrete peaks, is more plausible for free-electron-like materials, but does not adequately describe the maxima observed in other crystalline solids.

The inelastic scattering of excited electrons prior to emission into vacuum is a complicated process. The excited electrons may suffer inelastic scattering from one or more of a number of processes: (a) electron-electron scattering leading to electron-hole pair production via the screened-Coulomb interaction between excited and valence electrons, (b) collective electron excitations (surface and bulk plasmons), and (c) interaction with the lattice via electron-phonon scattering. For electrons with energies more than a few eV above the Fermi level, however, (a) and (b) constitute the dominant inelastic-scattering processes.[12] Surface-plasmon scattering is more probable than volume-plasmon scattering if the mean depth of escape is less than about 25 Å, [13] which is the case for SEE from metals and semiconductors.[2,14,15] Coupling with plasmons is likely to be less predominant, however, in all but the nearly-free-electron-like metals, [16] and even for these solids, photoelectron inelastic-scattering measurements on alkali metals[17] indicate pair production to be the major inelastic-scattering mechanism for kinetic energies $E_{kin} \lesssim 50$ eV.[18]

In Sec. II, we consider the distribution of secondary electrons to be a consequence of inelastic electron-electron scattering in which the predominant process is the population of final states by electron-hole pair production via screened-Coulombic interaction between the primary "hot" electrons and valence electrons in the solid.[12] The excited electrons undergo further inelastic-scattering events during transport to and escape from the surface, populating lower-energy final states in the process. The treatment can be generalized to include Auger-relaxation and plasmon-scattering processes. In view of the lack of any satisfactory rigorous treatment of low-energy ($E_p \lesssim 1$ keV) inelastic electron scattering by solid surfaces,[19] we review the multistep model (excitation, transport, and escape) used to describe inelastic scattering of photoelectrons, [20] and show that density-of-final-states features should be apparent in experimental SEE spectra of crystals.

Results are presented for graphite, which provide strong support for this view (Sec. III). Previous measurements[7] are extended and weak structure, resolved in the second derivative of the SEE energy-distribution spectrum, is reported for kinetic energies $10 \lesssim E_{kin} \lesssim 40$ eV, which correlates closely with emission associated with high density-of-states levels in the third-Brillouin zone. The analysis of such spectra requires a knowledge of the excited states at much higher energies than are usually covered by existing band-structure calculations. Consequently, in Sec. IV details are presented of a previous energy-band calculation[8] which is here refined and extended up to 55 eV above the Fermi energy. The calculated density of final states are compared in Sec. V with the observed SEE fine structure and show good agreement with the measurements. The role of interband transitions and selection rules in the initial absorption process are discussed in Sec. VI with reference to the energy-loss spectrum of the elastically reflected primary electrons. Finally, the major conclusions derived from this work are summarized in Sec. VII.

II. PAIR-PRODUCTION THEORY OF SECONDARY ELECTRON EMISSION

The distribution function $S_{ee}(E_p, E)$, for secondary electrons of energy E produced via electron-electron scattering by a primary electron of initial energy E_p, may be determined from the scattering rate for the production of electron-hole pairs using first-order time-dependent perturbation theory.[12] The transition probability per second for an electron in initial state $(E_p, \vec{k}_p)$ to be scattered down to a conduction state $(E_c, \vec{k}_c)$ and excite an electron up from a valence state $(E_v, \vec{k}_v)$ to state $(E_c', \vec{k}_c')$, thereby creating a hole in state $(E_v, \vec{k}_v)$, is

$$P = (2\pi/\hbar)\,|\langle \vec{k}_p, \vec{k}_v | M | \vec{k}_c, \vec{k}_c' \rangle|^2\, \delta(E_p + E_v - E_c - E_c'), \tag{1}$$

where $|\langle M \rangle|^2$ includes the matrix element of the perturbation Hamiltonian for the screened-Coulomb interaction. The process is illustrated in Fig. 1(a), all energies being with reference to the Fermi energy $E_F = 0$ eV. The Dirac δ function in Eq. (1) conserves energy, and momentum is conserved according to

$$\vec{k}_p + \vec{k}_v = \vec{k}_c + \vec{k}_c' + \vec{g}, \tag{2}$$

where $\vec{g}$ is a reciprocal-lattice vector. Kane[12] used this formalism to calculate the scattering rate for a "hot" electron to decay and produce an electron-hole pair in a semiconductor and obtained the result

$$\omega_{se}(E_p, E) = \frac{2\pi}{\hbar}\left(\frac{V}{(2\pi)^3}\right)^2 \sum_{n_p, n_c, n_v, n_c'} |\langle p, v | M | c, c' \rangle|^2$$

$$\times \frac{\int d\vec{k}_p\, d\vec{k}_c\, d\vec{k}_{c'}\ \delta(E_p - E)}{\sum\int d\vec{k}_p \delta(E_p - E)}$$
$$\times \delta(E_p + E_v - E_c - E_c'), \qquad (3)$$

where V refers to the volume of the unit cell, $|\langle M\rangle|^2$ is the matrix element of the screened-Coulomb interaction

$$M(p, v, c, c') \equiv \int \langle \psi_p(\vec{r}_1)\, \psi_v(\vec{r}_2)\, |(e^2/\epsilon|\vec{r}_1 - \vec{r}_2|)| \times \psi_c(\vec{r}_1)\, \psi_{c'}'(\vec{r}_2)\rangle\, d\vec{r}_1 d\vec{r}_2 \qquad (4)$$

including exchange, and ϵ is the frequency and momentum-dependent complex dielectric function $\epsilon(\omega, \vec{q})$, summed over all initial and final states with band indices n_p, n_c, n_v, and n_c'.

Kane[12] calculated the scattering rate for Si using Eq. (3) and found that the result was identical, within the statistical accuracy of the Monte Carlo method he used to evaluate the integrals in Eq. (3), to that obtained by neglecting $\vec{k}$ conservation. The "random-$\vec{k}$" approximation[20] follows if $\vec{k}_v$ in Eq. (1) is regarded as a random variable so that the probability of finding an electron with momentum $\vec{k}_v$ at energy E_v is proportional to the density of states, $N(E_v)$, i.e., $P(\vec{k}_v) = N_v(E_v)\, dE_v / \int N_v(E_v) dE_v = N_v(E_v)\, dE_v / 2N_u$, where N_u is the number of unit cells and the factor 2 is for spin. Assuming a constant "average" value of $|\langle M\rangle|^2$, independent of $\vec{k}$, one then obtains the scattering probability $P_s(E_p, E)$ for an electron with initial energy E_p to be scattered to energy E (per eV per second):

$$P_s(E_p, E) = N_c(E)\,(2\pi/\hbar)\,|\langle M\rangle|^2 \times \int_{-(E_p - E)}^{0} dE_v\, N_v(E_v)\, N_c(E_v + E_p - E), \qquad (5)$$

the conduction-band density of states $N_c(E)$ being the state degeneracy factor at energy E and temperature $T = 0\,^\circ$K.[21] The electron-electron scattering rate or total transition probability per second $\omega_{se}(E_p, E)$ for an electron with initial energy E_p is simply

$$\omega_{se}(E_p, E) = \int_0^{E_p} dE\, P_s(E_p, E), \qquad (6)$$

and the final-state energy-distribution function of secondary electrons of energy E produced by a primary electron of energy E_p is given by

$$S_{ee}(E_p, E) = \frac{2P_s(E_p, E)}{\omega_{se}(E_p, E)} = \frac{2N_c(E)\int_{-(E_p - E)}^{0} dE_v\, N_v(E_v)\, N_c(E_v + E_p - E)}{\int_0^{E_p} dE\left[N_c(E)\int_{-(E_p - E)}^{0} dE_v\, N_v(E_v)\, N_c(E_v + E_p - E)\right]} . \qquad (7)$$

The factor 2 in Eq. (7) arises from the fact that *two* secondary electrons are created in the pair-production process, $(E_c, \vec{k}_c)$ and $(E_c', \vec{k}_c')$[Fig. 1(a)] i.e., $\int_0^{E_p} dE\, S_{ee}(E_p, E) = 2$.

Secondary electrons can also be excited by the Auger process, which may be regarded as hole-hole scattering[20] [Fig. 1(b)], i.e., a hole $(E_h, \vec{k}_h)$, which is created in the valence band in the absorption process, scatters to an energy $(E_h', \vec{k}_h')$ through recombination and excites an electron-hole pair $(E_c, \vec{k}_c)$ and $(E_v, \vec{k}_v)$. The distribution function $S_{he}(E_h, E)$ for secondary electrons of energy E produced by a primary hole of energy E_h is[12,20]

$$S_{he}(E_h, E) = \frac{N_c(E)\int_{E+E_h}^{0} dE_v\, N_v(E_v)\, N_v(E + E_h - E_v)}{\int_0^{-E_h} dE\, N_c(E)\int_{E+E_h}^{0} dE_v\, N_v(E_v)\, N_v(E + E_h - E_v)} , \qquad (8)$$

where $\int_0^{-E_h} dE\, S_{he}(E_h, E) = 1$ in this case, since only *one* secondary electron with $E > E_F$ is produced.

The double fold of the one-electron density of states inside the integrals [Eqs. (5), (7), and (8)] produces a smeared-out background distribution of secondary electrons which, together with the escape function, results in the broad asymmetric "cascade peak" with its maximum a few eV above the vacuum level.[1] Final-density-of-states features appear superimposed on this background owing to the fact that $N_c(E)$ lies outside the integral sign.[16] We expect therefore to resolve conduction-band density-of-states structure in the experimental SEE spectrum, which is independent of the primary energy E_p.[22]

The dominant contribution to secondary emission in clean metals arises mainly from those electrons which have suffered a single inelastic electron-electron scattering event prior to escape from a surface region ~25 Å in depth.[14,15] A recent estimation[16] revealed that approximately 60% of electrons photoemitted from copper under 21.2-eV photon irradiation have been scattered once, 32% twice, and 6% three times during transport and escape from the surface. The number of once-scattered secondary electrons emitted per incident

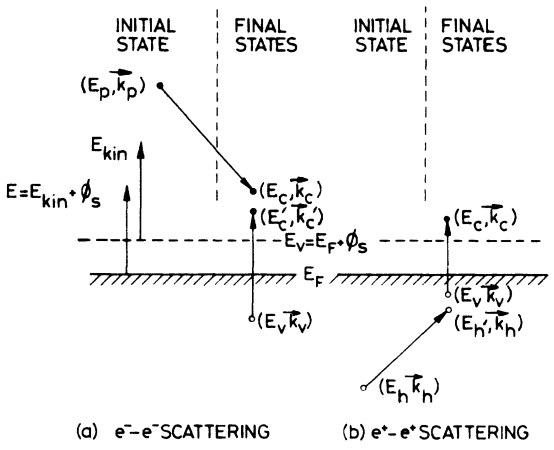

FIG. 1. Schematic diagram of secondary-electron excitation via electron-hole pair creation (Ref. 15). (a) Electron scattering: the primary electron is initially in conduction-band state $(E_p, \vec{k}_p)$, $E_p = E_c + E_c' - E_v$. (b) Hole scattering or Auger relaxation: the primary hole is initially in valence-band state $(E_h, \vec{k}_h)$, $E_h = E_h' + E_v - E_c$.

primary electron of energy E_p may be written[20]

$$D_s(E_p, E) = [1 - R(E_p)]T(E)f(E_v)[1 - f(E_c)] \times \int_{E_v}^{E_c} dE_c\, S_{ee}(E_p, E)\, P_0(E_p, E) \quad . \tag{9}$$

The factor containing the electron reflectivity $R(E_p)$ normalizes the distribution to the number of incident primary electrons initially injected into the solid. These "captured" electrons constitute a primary excited electron distribution $P_0(E_p, E)$ which, in a first approximation, may be regarded as the full characteristic energy-loss spectrum including thermal broadening of the incident monoenergetic electron beam.[22] At high primary beam energies ($E_p \gtrsim 75$ eV), the reflected primary-electron distribution (elastic peak together with the associated loss spectrum) does not overlap significantly and distort the "true" secondary distribution region of the observed spectrum given by $D_s(E_p, E)$ [Eq. (9)]. The Fermi distribution functions $f(E)$ guarantee filled initial and empty final states.

The particular form of the energy-dependent effective escape probability $T(E)$ depends on several simplifying assumptions.[20] For the case of specular surface scattering, it is defined in terms of an energy-dependent mean free path for inelastic scattering $L(E)$ and a surface transmission function $T_s(E)$, i.e., for excited electrons of energy $E > \phi_s$,

$$T(E) = T_s(E)\{\alpha L(E)/[1 + \alpha L(E)]\}\, C_1[\alpha(E), L(E), T_s(E)], \tag{10}$$

$$\left.\begin{aligned} T_s(E) &= 0 && \text{for } 0 < E < \phi_s \\ T_s(E) &= \frac{1}{2}\left[1 - \left(\frac{V_0}{V_0 + E - \phi_s}\right)^{1/2}\right] && \text{for } \phi_s < E \end{aligned}\right\} \tag{11}$$

where $\alpha(E)$ is an effective electron absorptivity term,[2] V_0 the inner potential of the solid, and C_1 is a factor which corrects for the fact that the excited electrons have randomly distributed momenta with respect to the surface normal.[20,23] The mean free path $L(E)$ for an excited electron with energy E is related to the electron-electron scattering rate $\omega_{se}(E_p, E)$ [Eq. (6)]

$$L(E) = L_0 \langle V_g(E) \rangle / \omega_{se}(E_p, E), \tag{12}$$

where L_0 is a normalization constant[20] and $\langle V_g(E) \rangle$ is an "average" group velocity.

For a "free electron" metal, the effective escape probability given by Eq. (10) is a smoothly varying function and nearly constant for electron energies $E \gtrsim \phi_s + 2$ eV.[20] The assumption of an "average" group velocity $\langle V_g(E) \rangle$ for excited electrons is a consequence of assuming all quantities in Eq. (9) to be independent of $\vec{k}$. The random-$\vec{k}$ approach [Eqs. (5)–(9)] is applicable to nearly-free-electron-like solids for which a simple pseudopotential works well, as was found for silicon.[12] Graphite is expected to behave similarly in this respect and give prominent one-electron final-density-of-states structure in the SEE spectrum. The scattering probability $\omega_{se}(E_p, E)$[Eq. (6)] is simply the reciprocal of the lifetime $\tau(E)$ for an electron at a final-state energy E. Lifetime broadening due to inelastic scattering will increase with energy away from the Fermi energy and fundamentally limits the sharpness of resolvable structure. More complex materials, such as the transition metals, require consideration of the detailed nature of the Coulomb matrix elements $|\langle M \rangle|^2$ [Eq. (4)] in view of the coupling between d-like and free-electron-like s states, and the $\vec{k}$ dependence of the group velocity $V_g(E, \vec{k})$. These factors may influence both the intensity and final-state energies of the emitted secondary electrons.[24] Electron-hole pair production due to plasmon-decay scattering processes can also conceivably result in the emission of secondary electrons.[10,11,25] These processes can be incorporated into Eq. (9) by suitably modifying the electron-electron scattering distribution function $S_{ee}(E_p, E)$ [Eq. (7)] and the energy-dependent mean free path (LE) [Eq. (12)]. Electron-hole pair inelastic-scattering processes are expected to give final-density-of-states features in the secondary electron distribution of graphite and the experimental results strongly confirm this view (Secs. III and V).

III. EXPERIMENTAL RESULTS

SEE spectra were recorded at 10^{-10} Torr vacuum for a primary-beam current of 1 μA incident at an angle θ to the c axis of a freshly-cleaved sample of highly-oriented, stress-annealed pyrolytic graphite.[7] The "back-scattered" secondary electrons were analysed using a standard hemispherical retarding-field three-grid analyser with an acceptance angle of 100°, details of which have been reported.[26] The large collection angle ensured that electrons excited and scattered within a large solid angle were detected. This, together with the fact that the secondaries suffer multiple elastic collisions with the lattice prior to emission, effectively sums over all $\vec{k}$ space with equal weight so as to approach closely the random-$\vec{k}$ approximation specified in Sec. II. "Elastic" electron-phonon scattering is expected to have a negligible effect on the final-state energies of secondary electrons for energies more than a few eV above the Fermi energy,[12] $E > \theta_s$.

The recorded spectra differ slightly from the theoretical distribution of emitted secondaries [Eq. (9)] in that the former is folded with an apparatus function which contains parameters such as the energy resolution of the grid system ($\simeq 1\%$), the thermal energy spread of the incident electron beam ($\simeq 0.2$ eV) and the modulation voltage. In previous measurements,[7] we reported well-resolved maxima in the secondary electron energy distribution of graphite for kinetic energies, $1 \lesssim E_{kin} \lesssim 20$ eV. The intensities of the spectral features were observed to decrease with increasing kinetic energy in agreement with high energy uv photoemission observations[27] of the energy dependent excitation strengths (proportional to the optical absorption cross-sections) from s-like and p-like initial states decreasing with increasing interband transition energy. Increasing lifetime broadening of these excited states also tends to smear-out any structure resolvable at higher energies.

In the present paper, we have extended the previous measurements by resolving extremely weak structure in the second-derivative spectrum of the energy distribution of secondary electrons emitted at kinetic energies up to 40 eV, using a modulation voltage of 1.5–2.5 V peak-to-peak amplitude superimposed on the analyzing-grids retarding voltage. The second-derivative SEE structure resolved at 11.5, 14.5, and 17.5 eV (Fig. 2) reproduces previously reported maxima resolved at 12.0, 14.5, and 17.5 eV in the energy distribution curve.[7] Some distortion of the peak locations (± 0.5 eV) can occur owing to the large modulation voltage amplitude required for the second-derivative spectra.[28] Structure due to discrete energy losses associated with the elastically reflected primary electrons (L) may be distinguished by comparison with the complete energy-loss spectrum (dashed line), which was obtained by energy modulating the electron beam only,[26] and by the fact that these maxima shift linearly in energy with varying primary beam energy E_p. In contrast, the location of the SEE maxima remain invariant with E_p as predicted by theory (Sec. II).[22] The energy-loss spectral structure (L) may also be completely suppressed for $E_p \gtrsim 50$ eV by modulating on both the incident-electron beam and the retarding grid voltages

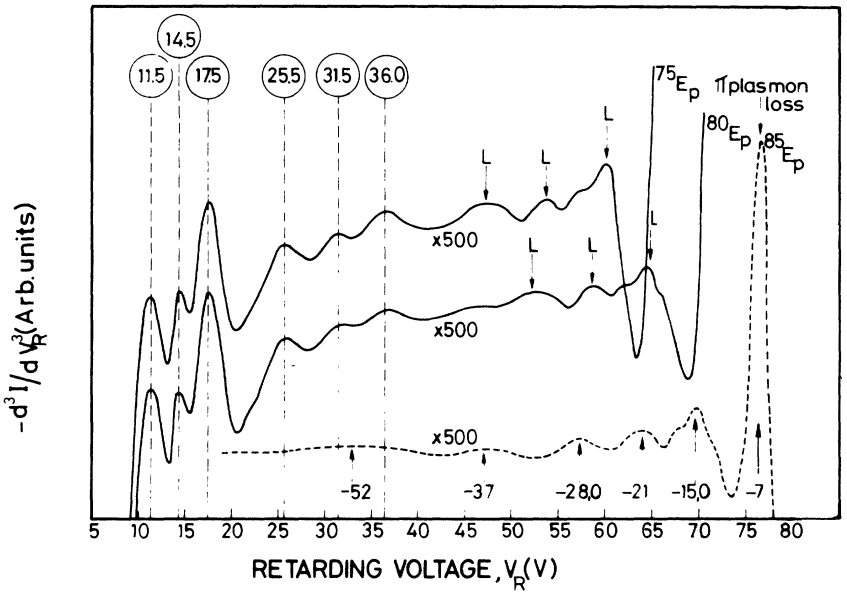

FIG. 2. Inverted second-derivative spectra, $-d^3I/dV_R^3$ vs V_R (full curves) of the SEE energy distribution, dI/dV_R vs V_R, for primary-beam energies $E_p = 75$, 80, and 85 eV, incident normal to the basal $(000\bar{1})$ plane of pyrolytic graphite. Discrete energy losses in the energy-loss spectrum (dashed curve) are labeled L, all curves recorded at 500× gain with reference to previously published spectra (Ref. 7).

simultaneously,[26] a technique which has proved useful for observing threshold excitation energies associated with SEE spectral features.[7]

The spectra shown in Fig. 2 were recorded at primary-beam energies, $E_p = 75$, 80, and 85 eV, the gain associated with each curve (500×) being with reference to previously published energy-distribution curves observed for $E_{kin} < 20$ eV and $30 \lesssim E_p \lesssim 150$ eV.[7] At lower primary-beam energies, $E_p \lesssim 30$ eV, the loss spectrum is difficult to suppress entirely owing to the increased oscillatory nature of the electron reflectivity[26] and distorts strongly the SEE spectrum. At higher primary-beam energies, $E_p \gtrsim 150$ eV, the electron cascade background increases considerably and limits the signal-to-noise ratio attainable. One aim of the present work was to look for final-state structure in the energy distribution of secondary electrons at sufficiently high kinetic energies, which could not be confused with possible one-electron–plasmon decay[10] or excitation[11] processes. The loss peaks, $L = 7$ and 28.0 eV (Fig. 2) are known to be associated with plasmon resonances in graphite.[29] It has been proposed[10] that plasmons could conceivably decay and excite electrons at the Fermi energy, which in graphite would give discrete secondary-electron structure emitted at kinetic energies of approximately 2.3 and 23.3 eV ($E_{kin} \simeq h\omega_p - \phi_s$, $\phi_s = 4.7$ eV). No such structure has been resolved at these energies, in agreement with the conclusions outlined in Sec. II. The energies of the SEE maxima show good agreement with the density-of-final-states histogram determined from the extended band structure, displayed for wave vectors in the $\vec{k}_z = 0$ plane of the hexagonal Brillouin zone of graphite (Fig. 3).

IV. HIGH-ENERGY BAND-STRUCTURE CALCULATION

Most calculations of the energy-band structure of graphite have been limited to states in the first- and second-Brillouin zones, emphasis being placed on accuracy over a relatively narrow energy range, 10–20 eV about the Fermi level, in order to explain the near uv optical properties.[30] For determining the uv optical properties in this energy range, a single-layer lattice model[9,30,31] seems reasonable, considering the large interlayer spacing (3.36 Å) compared with the interatomic spacing in a layer (1.42 Å). More detailed calculations using the four-atom unit cell of the multilayer crystal[8,32,33] verifies that this approximation is adequate for states within 10–15 eV of the Fermi level. For explaining infrared[34] and electrical properties, and Fermi surface topology,[32,34,35] however, it is necessary to account for the interaction among the layers. We find that the multilayer interaction is also important for obtaining an accurate band structure for states extending beyond 15 eV above the Fermi energy, because the higher conduction band states become diffuse and sensitive to details of the potential over the entire unit cell.

The model Hamiltonian and computational techniques used in this work have been discussed previously,[8] so that our description of the energy-band calculation will be brief. The discrete variational method[36] is very advantageous for treating a highly anisotropic crystal such as graphite, since there are no restrictions on the form of the crystal potential. Writing our effective one-electron model Hamiltonian in rydbergs, we have

$$H(\vec{r}) = -\nabla^2 + V_c(\vec{r}) + V_x(\vec{r}), \tag{13}$$

where $V_c(\vec{r})$ is the effective Coulomb self-consistent-field potential and $V_x(\vec{r})$ represents a local approximation to the exchange-correlation potential for an electron. The crystal potential is formed by a superposition of atomic Coulomb contributions from sites in the crystal,

$$V_c(\vec{r}) = \sum_{\zeta, i} v_i(\vec{r} - \vec{R}_\zeta - \vec{\mu}_i), \tag{14}$$

where $(\vec{R}_\zeta + \vec{\mu}_i)$ defines the position of the atom at site $\vec{\mu}_i$ within the unit cell at lattice site $\vec{R}_\zeta$. The Slater $\rho^{1/3}$ exchange approximation has been used

$$V_x(\vec{r}) = -6\beta\left[\left(\tfrac{3}{8}\pi \sum_{\zeta, i} \rho_i(\vec{r} - \vec{R}_\zeta - \mu_i)\right)\right]^{1/3}, \tag{15}$$

with β appearing as an exchange scaling parameter.

Approximate solutions to the Schrödinger equation can be obtained by a linear variational procedure in which we minimize the expectation values of the Hamiltonian by varying the coefficients in some fixed basis,

$$\psi_i(\vec{k}, \vec{r}) = \sum_j x_j(\vec{k}, \vec{r})\, C_{ji}(\vec{k}). \tag{16}$$

The Bloch basis set was constructed from the Slater-type orbitals listed in Table I. Orbitals with d symmetry on each atom site introduced no new states and contributed relatively little to the eigenvalues in this energy region and were not included in the basis set. In the calculation for the multilayer lattice, a total of 52 trial functions and 2400 integration points gave convergence of the levels in the third-Brillouin zone to ±0.8 eV for the σ bands and ±0.3 eV for the π bands. In order to achieve this convergence it was necessary to selectively choose which orbitals to include in the basis set. From the point of view of optimizing convergence, a first-principles muffin-tin band method would prove more efficient, but in graphite it would be necessary to include corrections arising from the non-muffin-tin potential terms.

In the discrete variational method, the matrix elements appearing in the resulting secular equations are evaluated by numerical quadrature over

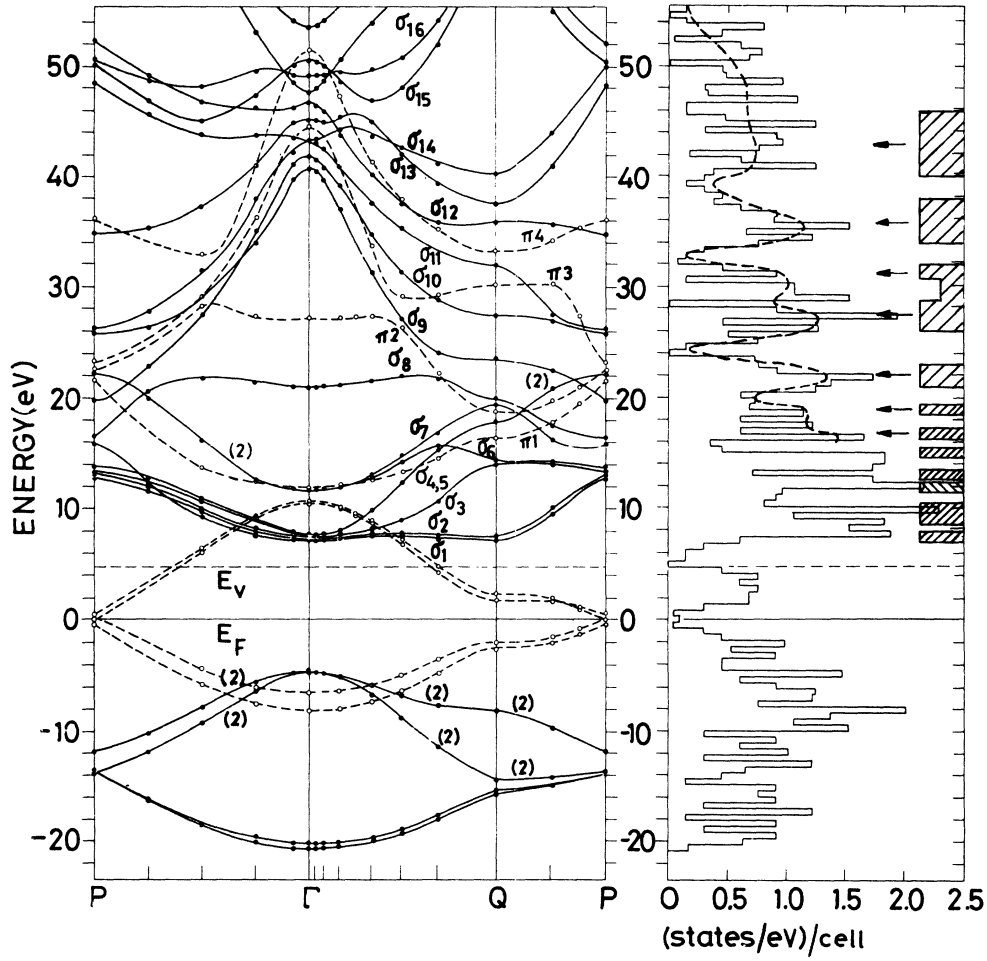

FIG. 3. High-energy band structure and density-of-states $N(E)$ histogram displayed for wave vectors in the $\vec{k}_z = 0$ plane of the hexagonal Brillouin zone of graphite. The electron states are identified as either σ (full curves) or π (dashed curves) and all states are singlet unless otherwise indicated. The energies and estimated half-widths of the SEE spectral features are indicated by the shaded block diagram; the doublet structure of the peak centered about 29 eV is indicated (see text). Fine structure in $N(E)$ is shown smoothed-out for states $E \gtrsim 15$ eV in view of the convergence of the higher excited states (± 0.8 eV) and lifetime broadening of the observed spectral structure. The energies of the secondary electrons are with reference to the Fermi level $E_F = 0$ (Ref. 38). $E_F - E_v = 4.7$ eV.

the crystal unit cell, e.g.,

$$H_{ij}(\vec{k}) = \sum_{m=1}^{M} w(\vec{r}_m)\, x_i^*(\vec{k}, \vec{r}_m)\, [H(r) x_j(\vec{k}, \vec{r})]_m , \qquad (17)$$

where $w(\vec{r}_m)$ is the weight function appropriate to the selected integration point density.

The potential used in this calculation was obtained directly from Eqs. (14) and (15) with an exchange parameter ($\beta = 0.76$) chosen to agree with earlier work.[8] The fact that the resulting band-structure features yield good agreement with experiment can be regarded as evidence for adequacy of the effective potential function. The energy bands for multilayer graphite are given in Fig. 3 for wave vectors in the basal plane of the Brillouin zone. For this investigation, calculations were carried out only for wave vectors in the plane $\vec{k}_z = 0$, since orbital modulation for $\vec{k}_z \neq 0$ generally leads to band splittings which are smaller than both the energy resolution of the experiment ($\simeq 1$ eV) and the accuracy of the computed eigenvalues.

The material is characterized by a set of partially overlapping σ and π bands with a valence band width of 20.7 eV. In the higher-energy region the conduction bands are considerably more complicated yielding a significant amount of structure in the calculated density of states.

A histogram representation of the density of states for the band structure was constructed according to the form

TABLE I. Atomic Slater-type orbitals (centered on each carbon site) used to construct Bloch basis set.

$1s$		$e^{-5.7r}$
$1s'$		$e^{-1.4r}$
$2s$		$re^{-1.4r}$
$2p_x$		x
$2p_y$		y $e^{-1.4r}$
$2p_z$		z
$2p'_x$		x
$2p'_y$		y $e^{-2.1r}$
$2p'_z$		z
$3s$		$r^2 e^{-1.4r}$
$3p_x$		x
$3p_y$	r	y $e^{-1.4r}$
$3p_z$		z

$$N(E) = \frac{2}{N_k \delta E} \sum_{j}^{N_k} \sum_{j=1} \Delta_j(\vec{k}_i), \tag{18}$$

where $\Delta_j(\vec{k}_i)$ is unity if the energy of band j at wave vector $\vec{k}_i$ is within δE of E, zero other wise, and j sums over all bands of interest. In this work, $N(E)$ appearing in Fig. 3 was calculated for $N_k = 144$ uniformly distributed sample wave vectors in the $\vec{k}_z = 0$ plane of the reduced Brillouin zone with a linewidth of 0.5 eV.

V. COMPARISON OF CALCULATED DENSITY OF STATES AND SEE FINE STRUCTURE

The energies of the SEE maxima (Fig. 2) shown arrowed in Fig. 3, and their width at half-maxima, indicated by the shaded block diagram, [37] show good agreement with the density of states maxima of the excited bands when corrected for the work functions of the sample and analyser grids (+4.7 eV), relative to the crystal Fermi level, $E_F = 0$ eV. [38,39] Maxima in $N(E)$ below 15 eV correlate closely with previously reported spectral structure observed at retarding voltages $V_R = 3.0$, 4.0, 7.5, 8.5, and 10.0 eV. [7]

The convergence of the higher excited states above 15 eV is considerably less (±0.8 eV) than that for the lower states (±0.1 eV), and thus no meaningful interpretation of the experimental data should be attached to the fine structure in the density of states histogram at these energies. To obtain a representation of $N(E)$ which is more compatible both with the experimental resolution and the convergence reliability of the calculation, $N(E)$ was formed over several different integration distributions of wave vectors in the Brillouin zone. Intercomparison of the stable structures in $N(E)$ then make it possible to form an average smoothed $N(E)$. This schematically smoothed $N(E)$ above 15 eV (dashed curve, Fig. 3) is more realistic to correlate with the observed spectral structure in view of the increased lifetime broadening of the high-energy excited states.

It is proposed that the maxima observed at retarding voltages of 11.5, 14.5, and 17.5 eV (Fig. 2) are due to electron emission from high density-of-final-states levels located at 16.2, 19.2, and 22.2 eV (Fig. 3). The 16.2-eV peak is determined by the critical point nature of the π_1 band about Q, enhanced by further critical point contributions from the σ_6, σ_7, and σ_8 bands along the symmetry direction QP. [40] Critical points in bands π_2, $\sigma_{4,5}$, σ_7, and σ_8, again about Q, effectively shape the 19.2-eV structure. The 22.2-eV peak is determined by the critical-point behavior of σ_9 at Q and transitions to the flat σ_8 band about the zone center.

A detailed analysis of contributions to the weak, broad peaks observed at higher retard voltages centered about 25.5, 31.5, and 36.0 eV in Fig. 2, is complicated by the large amount of fine structure in the density of states histogram and diffuseness of the bands in the third-Brillouin zone (Fig. 3). Nevertheless, details of the structure in $N(E)$ appear to cluster into more or less well separated groups, maxima in the "smoothed" curve coinciding closely with the observed spectral features centered about final-state energies 30.2, 36.2, and 41.2 eV relative to E_F. Some of the more prominent features of this fine structure have been resolved by increasing the gain and comparing the spectra observed for both 0° and 40° angles of incidence θ of the primary beam relative to the c axis of the crystal (Fig. 4). In particular, the broad peak centered at 25.5 eV (Fig. 2) is seen to split into two peaks at 24.5 eV and 26.5 eV retarding voltage (Fig. 4), when the crystal is rotated from $\theta = 0°$ to 40°. The origin of the SEE maxima observed at 24.5 eV (final-state energy, $E = 29.2$ eV) is the strong contribution to $N(E)$ at 27.5 eV due to the structure of the σ_{10} band about Q, enhanced by the flat π_2 band in an extended volume about the zone center. The 26.5-eV peak ($E = 31.2$ eV) arises from the π_3 band structure about Q at 30.5 eV.

This variation of the SEE peak intensities with incident angle θ, which is particularly apparent for incident beam energies close to the threshold energies for single electron excitations, $E_p \lesssim 50$ eV, [7,41] appears to be related to the strong selection rules which govern the allowed interband transitions in a strongly anisotropic material such as graphite. [9] Interpreted according to a simple band model of one-electron interband transitions [41] the absorption of primary electrons incident at an angle $\theta = 40°$ to the crystal $\vec{c}$-axis gives an *initial* population of final state "hot" electrons, the number excited being governed by selection rules for the excitations associated with polarization electric field vector $\vec{E}$ components both parallel and per-

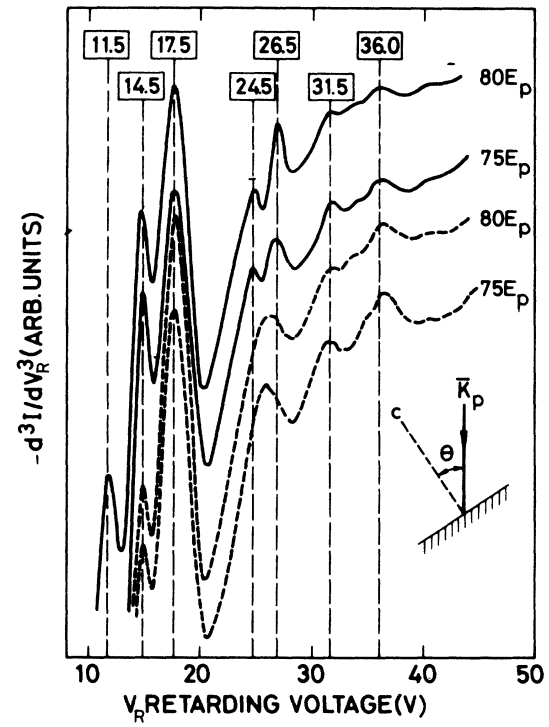

FIG. 4. SEE spectra similar to those in Fig. 2 at an increased gain of 1250× for primary-beam energies E_p = 75 and 80 eV and incident angles $\theta = 0°$ (dashed curve) and $\theta = 45°$ (full curve) relative to the crystal c axis. Note the doublet structure of the peak centered about 25.5 eV retard voltage when the crystal is rotated from $\theta = 0°$ to 40°, indicative of selection-rule-dependent interband transitions (see text).

pendicular to the crystal $\vec{c}$ axis. $\theta = 0°$ orientation results in $\vec{E} \parallel \vec{C}$ "optical-type" transitions only.[7,9,41] This point will be discussed further in Sec. VI.

The spectral structure at 31.5 eV (Figs. 2 and 4), $E = 36.2$ eV, correlates closely with maxima in $N(E)$ about 36.2 eV (Fig. 3) owing to structure in the σ_{12} and π_4 bands about Q and along the symmetry direction QP. This structure is broadened (Fig. 2) by the very weak shoulder resolved at 33 eV (Fig. 4) associated with the σ_{14} band minimum at Q. The SEE peak at 36 eV (Fig. 2), $E = 40.7$ eV, is determined by the σ_{14} minimum at Q, broadened by the structure of the σ bands about the zone center, the latter probably being the origin of the very weak peak barely resolved at 40 eV (Fig. 4).

VI. DISCUSSION

The agreement between the experimental results and the calculated final density of states provides support for the mechanism of secondary electron emission outlined in Sec. II, in which pair-production scattering is predominant. Emission associated with final-states maxima located in the third-Brillouin zone ($E \gtrsim 20$ eV) is approximately 100 times lower than that from states located near the vacuum level, $E_v = 4.7$ eV, as expected for decreasing energy-dependent interband excitation strengths.[27] At such high energies, the assumption of constant "averaged" matrix elements [Eqs. (5)–(9), Sec. II] is a valid approximation and any energy or $\vec{k}$ dependence of the matrix elements for electron-hole pair production is not expected to play a significant role in modulating the intensity of observed SEE fine structure. We observe, however, that the random-$\vec{k}$ approximation may be an over-simplification for an anisotropic crystal like graphite. The distribution function $D_s(E, E_p)$ [Eq. (9)] does not contain any matrix element but only the density of states and other quantities which are independent of $\vec{k}$. It offers no explanation therefore for the variation of intensity of the spectral features with orientation of the primary beam observed in this and previous work.[7,41]

Considering for a moment the matrix element of the screened-Coulomb interaction $|\langle M \rangle|^2$ [Eq. (4)], interband transitions will be sensitive to the direction of the local electric field vector $\vec{E}_{loc}$ in the solid, which is in turn determined by the nature of the dielectric screening.[15] The dielectric screening may be described by a frequency- and momentum-dependent complex dielectric constant $\epsilon(\omega, \vec{q})$ [Eq. (4)], which is tensorial in an anisotropic crystal such as graphite.[29] For this reason, whilst the nature of single-particle (and plasmon) excitations in cubic crystals are well-understood,[42] their detailed behavior in anisotropic media is complex.[29] Also, for low energy ($E_p \lesssim 100$ eV) inelastic electron scattering considered above, it is not possible to invoke linear-response theory in order to predict the nature of $\vec{E}_{loc}$.[15] The dielectric response of an anisotropic graphite crystal to a *fast* ($E_p \gtrsim 10$ keV) electron beam, however, has been shown to vary with angle of incidence of the approaching particle.[43] The initial coupling of the excitations to external probes such as light and fast electons has been considered[29] and strong selection rules shown to be operative.[9,43] In this context therefore it is relevant to consider briefly the energy-loss spectrum (Fig. 5).

The energy-loss intensity profile of crystals is dominated by plasmon losses for momentum transfer less than the "cut-off" wave vector $\vec{k}_c$. The probability for energy transfer ΔE to a single valence electron is reduced over that for a plasmon excitation by a factor $[(\Delta E/\hbar\omega_p)^3/(n_{av}/n)]f_{av}$, where the average oscillator strength $f_{av} < 1$ and the relative number of electrons in a band contributing to an interband transition is $n_{av}/n \ll 1$.[42] That is, in order for a discrete loss feature as-

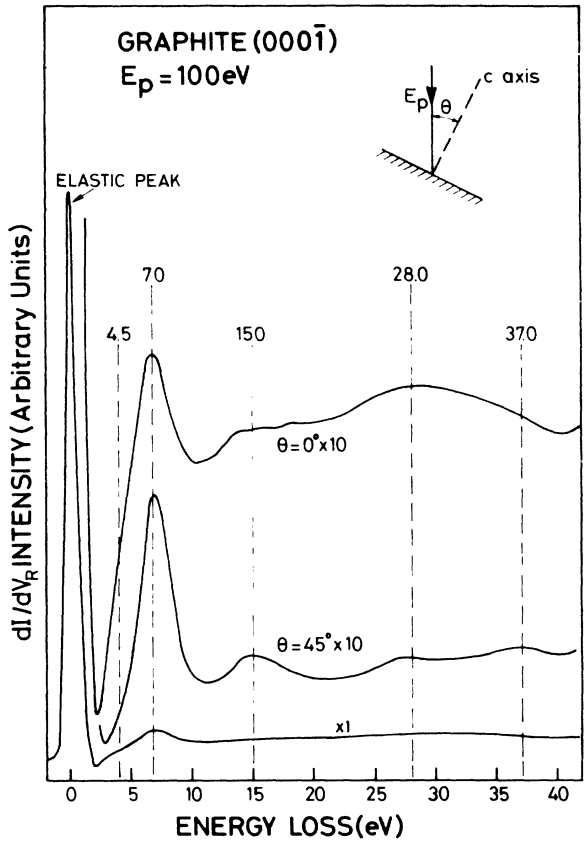

FIG. 5. Energy-loss intensity profile for primary electrons of energy $E_p = 100$ eV incident normal ($\theta = 0°$) and oblique ($\theta = 45°$) to the (000$\bar{1}$) basal plane surface of graphite. The spectra were recorded at 10× gain relative to the elastic peak (×1).

sociated with a particular one-electron transition to be resolved in the spectrum, the average oscillator strength f_{av} must be high for a specific ΔE value. This implies direct $\vec{k}$-conserving transitions reflecting *joint* density-of-states structure. Indirect transitions will tend to smear out resolvable structure to some extent. Both direct and indirect transitions are expected in low-energy electron scattering[19] owing to the possibility of momentum transfer to the excited electron by the incident electron. It is difficult therefore to relate structure in the loss spectrum with specific interband transitions, since the one-electron excitations tend to form an envelope profile owing to summation over energy and $\vec{k}$-space. The loss profile (Figs. 2 and 5) is dominated by the π-plasmon loss at 7.0 eV and the $(\sigma + \pi)$ "bulk" loss at 28 eV. Higher energy losses are usually attributed to multiple plasmon losses or combinations of plasmon and one-electron transitions.[6] While there is no obvious one-to-one correspondence between structure in the loss profile due to specific interband transitions and final-density-of-states features in the secondary-electron distribution, the over-all intensity of the loss profile is observed to vary with incident beam orientation θ (Fig. 5), in a manner analogous to SEE spectral intensity variations. This indicates that selection-rule-dependent matrix elements $|\langle M \rangle|^2$ [Eq. (4)] play a role in the production by interband transitions of excited electrons, produced during the absorption stage of the incident-electron beam owing to the tensor nature of the dielectric function ϵ, which determines the screened-Coulomb-interaction scattering process. This in turn implies that both the primary-excited-electron distribution $P_0(E_p, E)$ and the secondary-electron distribution $D_s(E_p, E)$ [Eq. (9)] will show some dependence on the direction of incidence of the primary-electron beam, as is observed.

VII. CONCLUSION

The approach adopted in the present work has been to consider the emission of secondary electrons as essentially a three-step inelastic photoelectric effect.[15,20] The absorption of the incident monoenergetic electrons is assumed to give a "primary" distribution of excited electrons, $P_0(E_p, E)$ [Eq. (9)], which will include those incident electrons which have been inelastically scattered and appear as the energy-loss spectrum.[22] Energy is transferred from the "primary" excited electrons to the valence electrons of the solid and, as first pointed out by Fröhlich[44] and later by Thomas,[15] as far as subsequent transport and escape processes are concerned the "true" secondary-electron distribution $D_s(E_p, E)$ [Eq. (9)] is independent of whether the energy absorbed by the target originates from an incident electromagnetic wave (photoemission) or from the Coulombic interaction with incident electrons (secondary-electron emission). As a consequence of inelastic electron-electron scattering, density of final states features are apparent in the secondary-electron and high-energy uv photoelectron[45] distribution spectra of crystals. The above results obtained for graphite provide evidence to support such a mechanism.

Further support for the view that final density of states structure is observed in secondary-electron-emission distributions is provided by the fact that similar spectral structure has been observed to evolve during the disordered-crystalline transition in amorphous C and Ge films.[46] The final-density-of-states distribution is particularly sensitive to the degree of short-range order present in highly-disordered solids,[47] and the observation of structure-dependent final states features in secondary-electron-energy distribution curves from such materials, endorses the general con-

clusions outlined in Sec. II, and the results in Sec. III and V. It is of interest to note that the Hartree-Fock-Slater model Hamiltonian with a Bloch wave description of the excited states (Sec. IV) apparently provides an adequate description of the high-energy band structure to the extent that positions of maxima in the density of final states correlate well with the observed SEE fine structure within the limitations imposed by lifetime broadening of the emitted electrons. A systematic study of the final density of states structure in SEE energy distributions of solids offers both a means of elucidating the nature of excited states and of testing the adequacy of the model Hamiltonian employed in energy-band calculations at high energies.

ACKNOWLEDGMENTS

We wish to express our gratitude to Dr. B. Feuerbacher and Dr. D. E. Ellis for stimulating discussions, and to D. K. Skinner for his expert technical assistance with the measurements.

---

*Research partially supported by U. S. Atomic Energy Commission under contract with Union Carbide Corp.

[1]P. A. Wolff, Phys. Rev. 95, 56 (1954).

[2]For comprehensive reviews of secondary-electron emission from solids, see A. J. Dekker, in *Solid State Physics*, edited by F. Seitz and D. Turnbull (Academic, New York, 1958), Vol. p. 251; O. Hachenberg and W. Brauer, in *Advances in Electronics and Electron Physics*, edited by L. Marton (Academic, New York, 1959), Vol. 11, p. 413.

[3]L. J. Haworth, Phys. Rev. 48, 88 (1935); R. Kollath, Ann. Phys. (Leipz.) 1, 357 (1947).

[4]J. J. Lander, Phys. Rev. 91, 1382 (1953).

[5]G. A. Harrower, Phys. Rev. 102, 340 (1956).

[6]E. J. Scheibner and L. N. Tharp, Surface Sci. 8, 247 (1967).

[7]R. F. Willis, B. Feuerbacher, and B. Fitton, Phys. Lett. A 34, 231 (1971); Phys. Rev. B 4, 2441 (1971).

[8]G. S. Painter and D. E. Ellis, Phys. Rev. B 1, 4747 (1970).

[9]F. Bassani and G. Pastori Parravicini, Nuovo Cimento 50 B, 95 (1967).

[10]C. V. von Koch, Phys. Rev. Lett. 25, 792 (1970).

[11]V. E. Henrich, Phys. Rev. B 7, 3512 (1973).

[12]E. O. Kane, Phys. Rev. 159, 624 (1967).

[13]G. D. Mahan, Phys. Status Solidi 55b, 703 (1973).

[14]H. Kanter, Appl. Phys. Lett. 10, 73 (1967); Phys. Rev. B 1, 522 (1970).

[15]H. Thomas, in *Proceedings of the International Symposium on Basic Problems in Thin Film Physics, Clausthal-Göttingen*, 1965 (Vandenhoeck and Ruprecht, Göttingen, 1966), p. 307.

[16]P. O. Nilsson and I. Lindau, in *Band Structure Spectroscopy of Metals and Alloys*, edited by D. J. Fabian and L. M. Watson (Academic, New York, 1973).

[17]N. V. Smith and W. E. Spicer, Phys. Rev. 188, 593 (1969).

[18]This is not to imply that plasmon-scattering processes do not contribute to secondary-electron emission. Coupling with plasmons during the emission of secondary electrons probably tends to reduce the intensities of the fine structure, particularly in free-electron metals. This would account for the weak intensities of the spectral features observed (see also Ref. 11).

[19]E. Bauer, Z. Phys. 224, 19 (1969).

[20]C. N. Berglund and W. E. Spicer, Phys. Rev. 136, 1030A (1964); D. E. Eastman in *Metals*, edited by R. F. Bunshah (Wiley, New York, 1972), Vol. 6, Chap. 6.

[21]The total secondary-electron emission yield of metals and semi-metals is relatively insensitive to temperature (Ref. 2), indicating that electron-phonon scattering constitutes a small effect compared with electron-electron scattering processes, which are dominant for the secondary-electron energies considered here.

[22]The factors under the integral signs [Eqs. (7) and (8)], provide a strong envelope factor which produces peaks in some curves, but since the energy location of such structure is *not* independent of the primary "hot" electron energy E_p, it is smeared-out and constitutes the featureless "cascade" background. "Primary" energy, E_p, referred to here includes all of those excited electrons which are produced in the solid owing to the initial absorption of monoenergetic incident electrons i.e., in a first approximation, the primary-electron distribution $P_0(E_p, E)$ will include those incident electrons which have been inelastically scattered by plasmons as well as interband transitions, i.e., $P_0(E_p, E)$ will include the full energy-loss spectrum, so that E_p is variable (see text).

[23]H. W. Streitwolf, Ann. Phys. (Leipz.) 3, 183 (1959).

[24]N. E. Christensen, Phys. Status Solidi 55b, 117 (1973).

[25]G. F. Amelio, J. Vac. Sci. Technol. 7, 593 (1970); A. Rothwarf, J. Appl. Phys. 44, 752 (1973).

[26]D. K. Skinner and R. F. Willis, Rev. Sci. Instrum. 43, 731 (1972).

[27]D. E. Eastman, and M. Kuznietz, Phys. Rev. Lett. 26, 846 (1971).

[28]Structure in the secondary-electron energy distribution curve reported previously (Ref. 7) was resolved at relatively low gain (1–10×) using peak-to-peak voltage modulation amplitudes $\lesssim$1 V.

[29]E. Tosatti, in *Proceedings of Enrico Fermi International Summer School of Physics on Atomic Structure and the Property of Solids, July* 1971, edited by E. Burstein (Academic, New York, 1972); Nuovo Cimento 63B, 54 (1969).

[30]D. L. Greenaway, G. Harbeke, F. Bassani, and E. Tosatti, Phys. Rev. 178, 1340 (1969).

[31]F. J. Corbato, in *Proceedings of the Third Carbon Conference* (Pergamon, London, 1959), p. 173.

[32]E. Doni and G. Pastori Parravicini, Nuovo Cimento 64B, 117 (1969).

[33]M. Tsukada, K. Nakao, Y. Uemura, and S. Nagai, J. Phys. Soc. Jap. 32, 54 (1972).

[34]L. G. Johnson and G. Dresselhaus, Phys. Rev. B 7, 2275 (1973).

[35]J. W. McClure, Phys. Rev. 108, 612 (1957); G. Dresselhaus and M. S. Dresselhaus, Phys. Rev. 140, A401 (1965).

[36]D. E. Ellis and G. S. Painter, Phys. Rev. B 2, 2887 (1970).

[37]The observed widths of the maxima in the second derivative spectra (Figs. 2 and 4) are approximately 50% of that in the energy distribution if a Lorentzian line shape

is assumed for these energies.

[38]The work functions of the sample $\phi_s = 4.7$ eV and of the stainless-steel grids, $\phi_g = 4.4$ eV (Ref. 39), must be taken into account in determining the absolute energies of the emitted electrons. Since the sample and analyzing grids are referenced at their Fermi levels, zero retarding voltage $V_R = 0$ corresponds to an energy $E = \phi_g$. The low-voltage cut-off of the measured SEE distribution is determined by the sample vacuum level which occurs at $V_R = \phi_s - \phi_g = +0.3$ eV. In the present measurements, the retard voltages, at which SEE fine structure was observed, were corrected to obtain absolute energies E relative to the graphite-sample Fermi energy by adding the factor $(\phi_g + 0.3) = 4.7$ eV. $E_{\text{kin}} \equiv E - \phi_s$ (Fig. 1).

[39]B. Feuerbacher and B. Fitton, J. Appl. Phys. 43, 1563 (1972).

[40]The term "critical-point contribution" is used here in its broadest sense to include not only van Hove singularities at symmetry points at which the group velocity is zero, as assumed in the earlier work (Ref. 7), but to include contributions from extended regions of $\vec{k}$-space corresponding to flat final bands, $\nabla_{\vec{k}}[E_c(\vec{k})] = 0$.

[41]R. F. Willis and B. Fitton, J. Vac. Sci. Technol. 9, 651 (1972).

[42]D. Pines, Rev. Mod. Phys. 28, 184 (1956).

[43]K. Zeppenfeld, Phys. Lett. A 25, 335 (1967); Z. Phys. 211, 391 (1968).

[44]H. Fröhlich, Proc. Phys. Soc. (Lond.) 68, 657 (1955).

[45]A. D. Baer and G. P. Lapeyre, Phys. Rev. Lett. 31, 304 (1973).

[46]R. F. Willis, L. D. Laude, and B. Fitton, Phys. Rev. Lett. 29, 220 (1972); R. F. Willis, B. Fitton and D. K. Skinner, J. Appl. Phys. 43, 4412 (1972).

[47]B. Kramer in *Festkörperprobleme XII, Advances in Solid State Physics*, edited by O. Madelung (Pergamon, Vieweg, 1972), p. 133.